HHS Public Access

Author manuscript

Brain Res Bull. Author manuscript; available in PMC 2021 August 01.

Published in final edited form as:

Brain Res Bull. 2020 August ; 161: 106–115. doi:10.1016/j.brainresbull.2020.05.004.

Transient Gain of Function of Cannabinoid CB_1 Receptors in the Control of Frontocortical Glucose Consumption in a Rat Model of Type-1 Diabetes

Joana Reis Pedro[a,$,1], **Liane I. F. Moura**[a,$,1], **Ângela Valério-Fernandes**[a,§,1], **Filipa I. Baptista**[b], **Joana M. Gaspar**[a,$], **Bárbara S. Pinheiro**[a,$], **Cristina Lemos**[a,$], **Fernanda Neutzling Kaufmann**[a,$], **Carla Morgado**[c,$], **Carla S. da Silva-Santos**[a,$], **Isaura Tavares**[c,§], **Samira G. Ferreira**[a], **Eugénia Carvalho**[a,§], **António F. Ambrósio**[a,§], **Rodrigo A. Cunha**[a,§], **João M.N. Duarte**[d], **Attila Köfalvi**[a,§,*]

[a]CNC - Center for Neuroscience and Cell Biology, University of Coimbra, 3004-504 Coimbra, Portugal;

[b]Coimbra Institute for Clinical and Biomedical Research, Faculty of Medicine, University of Coimbra, 3000-548 Coimbra, Portugal;

[c]Department of Biomedicine, Faculty of Medicine, University of Porto, Porto, Portugal;

[d]Department of Experimental Medical Science, Faculty of Medicine, Lund University, Lund, Sweden; Wallenberg Centre for Molecular Medicine, Lund University, Lund, Sweden;

Abstract

Here we aimed to unify some previous controversial reports on changes in both cannabinoid CB_1 receptor (CB_1R) expression and glucose metabolism in the forebrain of rodent models of diabetes. We determined how glucose metabolism and its modulation by CB_1R ligands evolve in the frontal cortex of young adult male Wistar rats, in the first 8 weeks of streptozotocin-induced type-1

[*]Corresponding author at: CNC - Center for Neuroscience and Cell Biology, University of Coimbra, 3004-504 Coimbra, Portugal.

[$]Present addresses: VIB Discovery Sciences, Bio-incubator Leuven, 3001 Leuven (Heverlee), Belgium (J.R.P.); Research Institute for Medicines (iMed.ULisboa), Faculty of Pharmacy, Universidade de Lisboa, Av. Professor Gama Pinto, Lisbon 1649-003, Portugal (L. I. M.); Post-Graduation Program in Biochemistry, Federal University of Santa Catarina, Florianópolis, Brazil (J.M.G.); Experimental Psychiatry Unit, Center for Psychiatry and Psychotherapy, Medical University Innsbruck, Austria (B.S.P and C.L.); Department of Psychiatry and Neuroscience, Faculty of Medicine and CERVO Brain Research Center, Université Laval, Quebec City, Canada (F.N.K.);

[§]Additional affiliations: I3S Instituto de Investigação e Inovação em Saúde, Universidade do Porto, Portugal and IBMC - Instituto de Biologia Molecular e Celular, Universidade do Porto, Portugal (I.T.); The Portuguese Diabetes Association (APDP), Lisbon, Portugal (E.C.); Arkansas Children's Research Institute, and Department of Geriatrics, University of Arkansas for Medical Sciences, Arkansas 72205, United States (E.C.); Faculty of Medicine, University of Coimbra, 3004-504 Coimbra, Portugal (R.A.C); Institute for Interdisciplinary Research, University of Coimbra, 3030-789 Coimbra, Portugal (A.V-F.; E.C.; A.K.);

[1]These authors contributed to this paper equally.

Author Contributions: Conceptualization, A.K.; methodology, all authors.; animals (purchase, diabetes induction, monitoring):, L.I.F.M., J.M.G., F.I.B., B.S.P., C.L., C.S.S-S., F.N.K., C.M., I.T., A.F.A., J.M.N.D., R.A.C.; resources, funding, A.K., I.T., A.F.A., R.A.C., E.C.; data curation, A.K.; uptake experiments: J.R.P., A.K., A.V.-F., B.S.P., C.L., C.S.S-S., F.N.K., Western blotting: L.I.F.M., J.M.G., F.I.B., S.G.F., J.M.N.D., E.C.; A.F.A.; PCRs: J.M.N.D., first draft, A.K.; final version, all authors.

Conflicts of Interest: The authors declare no conflict of interest. The funding agencies had no role in the design of the study; in the collection, analyses, or interpretation of data; in the writing of the manuscript, or in the decision to publish the results.

diabetes (T1D). We report that frontocortical CB_1R protein density was biphasically altered in the first month of T1D, which was accompanied with a reduction of resting glucose uptake *ex vivo* in acute frontocortical slices that was normalized after eight weeks in T1D. This early reduction of glucose uptake in slices was also restored by *ex vivo* treatment with both the non-selective CB_1R agonists, WIN55212–2 (500 nM) and the CB_1R-selective agonist, ACEA (3 μM) while it was exacerbated by the CB_1R-selective antagonist, O-2050 (500 nM). These results suggest a gain-of-function for the cerebrocortical CB_1Rs in the control of glucose uptake in diabetes. Although insulin and IGF-1 receptor protein densities remained unaffected, phosphorylated GSKα and GSKβ levels showed different profiles 2 and 8 weeks after T1D induction in the frontal cortex. Altogether, the biphasic response in frontocortical CB_1R density within a month after T1D induction resolves previous controversial reports on forebrain CB_1R levels in T1D rodent models. Furthermore, this study also hints that cannabinoids may be useful to alleviate impaired glucoregulation in the diabetic cortex.

Keywords

cannabinoid CB_1 receptor; cerebral glucose metabolism; type-1 diabetes; frontal cortex; Goto-Kakizaki rat; Wistar rat

1. Introduction

Marihuana has long been known to modulate carbohydrate metabolism in animal models (de Pasquale et a., 1978) and man (Benowitz *et al.*, 1976). One of the major targets of marihuana's Δ^9-THC in the body is the cannabinoid CB_1 receptor (CB_1R), the foremost metabotropic receptor of the endocannabinoid system, and is widely expressed in most mammalian organs and tissues, including the CNS, the pancreas, the liver and the skeletal muscle (Katona and Freund, 2012; Solymosi and Köfalvi, 2017). The CB_1R is a major regulator of the body's energy homeostasis, via three major targets: neural circuits, neurohumoral communication and cellular metabolism (Piazza et al., 2017; Ruiz de Azua et al., 2019).

Overactivation of the endocannabinoid system may lead to systemic insulin resistance (Bowles et al., 2015; Jourdan et al., 2017; Sidibeh et al., 2017), which is a primary pathomechanism of diabetes. One theory suggests that the CB_1R inhibits insulin receptor signaling via physical complexing, that is, heteromerization (Dalton and Howlett, 2012; Kim et al., 2012). Indeed, we found in the rat nucleus accumbens that the CB_1R co-immunoprecipitates with the insulin receptor, and its activation prevents insulin from stimulation of [^{3}H]deoxyglucose uptake (Pinheiro et al., 2016). Interestingly, the interaction between insulin and endocannabinoids is even more intricate. For instance, insulin stimulates endocannabinoid release in the ventral tegmental area (Labuèbe et al., 2013), while the CB_1R stimulates insulin secretion in the endocrine pancreas (Bermúdez-Silva et al., 2016). This heralds the possibility that diabetes could be associated with alterations in CB_1R signaling.

Our particular area of interest is the cerebral cortex because of the widely accepted but little understood link between systemic metabolic diseases and neurodegeneration (Duarte, 2015;

Rehni et al., 2018). It has been speculated that cerebral dysmetabolism can contribute to the onset of brain disorders (de Ceballos and Köfalvi, 2017; Zilberter and Zilberter, 2017), prompting the interest to identify new pharmacological targets to mitigate brain dysmetabolism. Recently we reported that untreated type-1 diabetes (T1D) triggered a reduction both in CB_1R density and in glucose uptake in hippocampal and frontocortical slices of mice. Furthermore, the genetic deletion of the CB_1R also caused similar glucose dysmetabolism, but strikingly, no further impairment was observed in the diabetic CB_1R knockout animals (Moura et al., 2019). This strongly suggests that CB_1R dysfunction may mediate some deleterious effects of T1D on brain glucose metabolism.

We now used *ex vivo* frontocortical tissue from control and diabetic rats to compare glucose metabolism, CB_1R density, and the effect of CB_1R ligands at 2, 4 and 8 weeks after a single i.p. injection with streptozotocin (STZ) or vehicle. We found that all the investigated parameters significantly change according to the time-course of the disease and that acute *ex vivo* CB_1R stimulation may prevent early dysregulation of glucose metabolism in the frontocortical slices.

2. Materials and Methods

2.1. Animals and diabetes models

All studies were conducted in accordance with the principles and procedures outlined as "3Rs" in EU guidelines (86/609/EEC), FELASA, and the National Centre for the 3Rs (the ARRIVE; Kilkenny et al., 2010), and were approved by the Animal Care Committee of the Center for Neuroscience and Cell Biology of the University of Coimbra, Portugal. We also applied the ARRIVE guidelines for the design and execution of *in vitro* experiments (see below), as well as for data management and interpretation (McGrath et al., 2010).

Eighty two male Wistar Han rats (10-week-old) were purchased from Charles River (France) and housed in a temperature and humidity-controlled environment with 12 h light on/off cycles and ad libitum access to food and water. All efforts were made to minimize the number of animals used and to minimize their stress and discomfort.

Fifty two rats were randomly assigned to sham- and STZ-injected groups. These groups were further randomly stratified into 3 subgroups, which were kept alive for 2, 4 and 8 weeks post-injection. At 12 weeks of age, type-1 diabetes mellitus (T1D) was induced with one single intraperitoneal (i.p.) injection of 60 mg/kg streptozotocin (STZ) (Szkudelski, 2001), after four hours of food deprivation. STZ was kept at −20°C until use, and its solution was freshly prepared in citrate buffer (10 mM; pH 4.5) less than 10 min before i.p. injection. Control rats were injected with the vehicle, citrate buffer, and maintained under the same conditions as the treated ones. Both body weight and blood glucose levels were measured both before and 3 days after STZ injection as well as on the day of sacrifice (*i.e.* 2, 4 and 8 weeks post-STZ injection) from tail vein blood with the glucose oxidase method, using a glucometer and reactive test stripes (Elite-Bayer SA, Portugal) (SFig. 1). Rats with blood glucose levels higher than 250 mg/dL were considered diabetic (de Morais et al., 2016).

We also had access to freshly isolated cortex for Western blotting and real-time PCR from 5-month-old male Goto-Kakizaki rats (Taconic, Lille Skensved, Denmark) – a model for type 2 diabetes mellitus (T2D), which spontaneously develops insulin resistance without obesity. For control, we used age-matched Wistar-Hannover-Galas rats (also from Taconic).

2.2. In vitro *tandem [^{3}H]DG and [^{14}C]-glucose uptake in brain slices*

This assay was carried out now on frontocortical slices as before on hippocampal and accumbal slices (Lemos et al., 2012; Pinheiro et al., 2016), with slight modifications after optimization. Sections 1.2 and 2.1 of the Supplemental File contain the detailed description of the optimization process of the *in vitro* tandem [^{3}H]DG/[^{3}H]MG and [^{14}C]-glucose uptake in cerebrocortical slices. The optimization process determined that [^{3}H]DG rather than [^{3}H]MG is the suitable “stable” analogue for a 30-min-long glucose uptake assay in cortical slices, after 60 min recovery. The following optimized methods correspond to the experiments presented here under Sections 3.1. and 3.2. of the Results.

Before decapitation with a stainless steel guillotine, the rats were deeply anesthetized with 2-bromo-2-chloro-1,1,1-trifluoroethane (halothane; 5%, 1 L/min flow rate in an induction chamber), thus showed no reaction to tail pinch and handling while still breathing. The brains were quickly removed and the cortices were dissected in ice-cold Krebs-HEPES assay medium of the following composition (in mM): NaCl 132, KCl 3, KH_2PO_4 1.2, $MgSO_4$ 1.2, $CaCl_2$ 2.5, $NaHCO_3$ 25, glucose 3, HEPES 10 (pH 7.4). Subsequently, 400 μm-thick coronal cortical slices were cut with the help of a McIllvain tissue chopper (the Mickle Laboratory Engineering Co. Ltd), then the slices were collected in a 50 mL pregassed (by 5% CO_2, 95% O_2) and prewarmed (to 37 °C) Krebs-HEPES assay medium (aka. recovery bath). Each holding chamber contained six submerged baskets, which are 15 mm tall and 10 mm wide, and have a 80 μm-pore nylon mesh bottom. This setup allows freely transferring and batch incubating slices up to ~5 mg protein/well in a 50 mL bath.

The pool of slices from each rat was divided into four holding chambers. In the same experiment, frontocortical slices from both sham and diabetic rats were co-incubated in the same holding chambers (although, in separate baskets) to increase statistical power. After 55 min incubation (recovery period) under gentle gassing at 37 °C, chamber 3 received the synthetic cannabinoid agonist, WIN55212–2 (final concentration: 500 nM) or when noted, the synthetic CB_1R-selective agonist, ACEA (3 μM), chamber 4 received the CB_1R-selective neutral antagonist, O-2050 (500 nM), and chambers 1 and 2 received the vehicle DMSO (0.1%). The concentrations of the cannabinoids were selected based on a previous review (Solymosi and Köfalvi, 2017). Four min later, chamber 2 received 263 μL of a 3 M KCl solution to create the depolarized condition (final K^+ concentration: 20 mM), while the rest of the chambers received an equivalent amount of NaCl serving as osmotic control. One min later, [^{3}H]DG (1 nM) and [^{14}C]$_6$-glucose (50 nM) were bath-applied in the chambers (for more information on the radiochemicals, see Supplemental File). Thirty min later, the baskets with the slices were transferred to large volumes of ice-cold assay medium for extensive washing, and then the slices were removed to 1 mL of NaOH (0.5 M) to determine the uptake of the tracers and protein quantities. Original bath samples were also counted to

measure the precise concentrations of the two radiotracers. For calculations, see Supplemental File.

2.3. Western blotting

The remaining frontocortical slices from each rat were used for total membrane extraction: The tissue was homogenized at 4 °C in sucrose (0.32 M) – HEPES (15 mM) buffer (pH: 7.4). The homogenate was centrifuged at 3,000 g for 10 min at 4 °C. The supernatant was then resuspended in a solution of 50 mM Tris and 10 mM $MgCl_2$ (pH 7.4), centrifuged at 28,000 g for 20 min at 4 °C. From the resulting pellet, proteins were extracted with RIPA buffer (50 mM Tris/HCl [pH 8.0], 150 mM NaCl, 1% Nonidet P-40, 0.5% sodium deoxycholate, 0.1% sodium dodecyl sulfate (SDS), 2 mM EDTA, proteases inhibitor cocktail, phosphatase inhibitor cocktail and 1 mM dithiothreitol) and these protein lysates were denatured at 95 °C, for 5 min, in sample buffer (0.125 mM Tris [pH 6.8], 2% w/v SDS, 100 mM dithiothreitol, 10% glycerol and bromophenol blue). Thirty μg of total protein was resolved on 10% SDS-PAGE and transferred to polyvinylidene difluoride membranes. The membranes were blocked with 5% (w/v) fat-free dry milk in Tris-buffered saline containing 0.1% (v/v) Tween 20, for 1 h at room temperature.

After blocking and washing, membranes were incubated overnight at 4°C with the primary antibodies against the different proteins studied (for their suppliers, see *2.6. Materials*): IRβ (1:1000), IGF-1R (1:1000), p-GSK3α (1:1000), GSK3α (1:1000), p-GSK3β (1:1000), GSK3β (1:1000), CB_1R (1:1000), and β-actin (1:1000). After incubation, membranes were washed and incubated for 1 h at room temperature, with alkaline phosphatase-conjugated anti-rabbit, anti-guinea pig or anti-mouse antibody (Santa Cruz Biotechnology; all at 1:5000). The membranes were exposed to ECF reagent followed by scanning for blue excited fluorescence on the VersaDoc (Bio-Rad Laboratories). The generated signals were analyzed using the Image-Quant TL software, and the background for each individual band was sampled adjacent to each bar. Density values were normalized to β-actin and these normalized values of the diabetic rats were again normalized to each WT sham normalized values in the same membrane.

2.4. Real-time PCR

Rat cortex samples were freshly isolated and immediately frozen in liquid nitrogen. Total RNA was extracted from these tissue samples with MagNA Lyser Instrument and MagNA Pure Compact RNA Isolation kit (Roche, Portugal) according to the manufacturer's instructions. Reverse transcription for first-strand cDNA synthesis from each sample was performed using random hexamer primer with the Transcriptor First Strand cDNA Synthesis kit (Roche) according to manufacturer's instructions. Resulting cDNAs were used as template for real-time PCR, which was carried out on LightCycler instrument using the FastStart DNA Master SYBR Green I kit (Roche) and the primers (Tib MolBiol, Germany) listed in Table 1.

Quantification of mRNA in the samples was carried out on the basis of standard curves run simultaneously. The cDNA standards for the calibration curve were generated by conventional PCR amplification (Table 2). The PCR products were run in a 3% agarose gel

electrophoresis to verify fragment size and the absence of other contaminant fragments, quantified by absorbance at 260 nm, and serially diluted to produce the standard curve (100 to 108 copies/μL). Each real-time PCR reaction was run in triplicate and contained 2 μL of cDNA template, 0.3 μM of each primer, and 3 or 3.5 mM $MgCl_2$ (see Table 2), in a reaction volume of 20 μL. Cycling parameters are described in Table 2. The analysis of melting curves ensured that only a single product was amplified. The expression of mRNA was calculated relative to β-actin mRNA expression.

2.5. Data handling

For data presentation and manipulation, we followed the rules of Curtis et al. (2015). All data represent the mean and S.E.M. of $n \geq 5$ individual observations (animals). Means were tested for normality with the Kolmogorov-Smirnov test. Statistical significance was determined by one-way ANOVA of repeated measures followed by Bonferroni's post-hoc test or two-tailed Student's t-test (except where noted otherwise), and $P < 0.05$ was accepted for significant difference, according to Curtis et al. (2015). Tests were performed and figures were prepared using the GraphPad Prism 5.0 software package.

2.6. Materials

The antibodies against phospho-(p)-(Ser21) glycogen synthase kinase α (GSK3α), total and p(Ser9)-GSK3β, total and p(Ser473)-Akt, were purchased from Cell Signaling Technologies (Danvers, MA, USA). The antibodies against the β chain of the insulin receptor (IR) and the insulin-like growth factor receptor (IGF-1R) were purchased from Santa Cruz Biotechnology (Santa Cruz, California, USA). The antibody against total GSK3α was obtained from UpState (Lake Placid, NY) and the antibody against β-actin was bought from BioLegend (San Diego, CA). The guinea-pig anti-CB_1R antibody was obtained from Frontier Institute co., ltd. (Hokkaido, Japan), and we have tested its selectivity before (Bitencourt et al., 2015). The chemifluorescence (ECF) reagent was acquired from GE Healthcare (Chalfont St. Giles, UK). 2-deoxy-2-(3-(methyl-3-nitrosoureido)-D-glucopyranose (streptozotocin or STZ) and other unspecified (in)organic reagents were from Merck (formerly, Calbiochem, Sigma-Aldrich, Merck-Millipore Corporation; Darmstadt, Germany).

3. Results

3.1. Glucose uptake in frontocortical slices of diabetic rats

The subjects of the following assay are rats in which diabetes was elicited with 1 single i.p. injection of STZ at 12 weeks of age, together with their sham-injected controls. SFig. 1 documents that the STZ-injected rats became in fact diabetic. The sham rats showed steadily increasing body weight, while the STZ-injected rats showed a reverse tendency. Blood glucose levels were highly elevated in the diabetic animals.

The following assay was carried out in pairwise manner, that is, randomly chosen slices of one sham and one diabetic animal were simultaneously incubated in four common holding chambers (besides an extra chamber on ice to measure external non-specific [^{3}H] and [^{14}C] labeling). The age of the sham animals (*i.e.* the fact that they were sacrificed at 14, 16 and

20 weeks of age) did not significantly affect glucose uptake under either resting conditions or high-K^+ depolarization (Fig. 1), although there was a nearly significant tendency ($P = 0.05–0.1$) for higher glucose uptake under high-K^+-depolarization in slices from diabetic rats, relative to their own control (Fig. 1D). The rationale behind evaluating resting and depolarized glucose consumption is to compare two extreme conditions. Under prolonged depolarization, the brain slices are submitted to an extreme energetic stress similar to an epileptic activity *in vivo* which can unveil additional impairments. In contrast, the basal uptake probably correlates better with what is seen in human subjects resting under a [^{18}F]-FDG-PET scan, even if this is speculative. In the sham animals, only depolarization affected significantly glucose uptake, while the synthetic CB_1R ligands, – as we previously published in the hippocampus (*e.g.* Lemos et al., 2012) were devoid of effect on glucose uptake in the resting slice.

Two weeks post-STZ injection, rat cortical slices exhibited a 15.2 ± 3.9% decrease in resting glucose uptake (diabetic DMSO control; $n = 14$, $P < 0.01$; as assessed with repeated measures ANOVA on the raw data) (Fig. 1A), which was normalized by treatment of the slices with the non-selective cannabinoid agonist, WIN55212–2 (500 nM; $P > 0.05$ vs. DMSO). To certify that the effect of WIN55212–2 is CB_1R-dependent, we have also tested the CB_1R-selective agonist, ACEA (3 μM) (Hillard et al., 1999) in a new batch of 2 × 6 rats. ACEA had no significant effect on *ex vivo* cortical glucose uptake in the sham-injected rats (95.2 ± 11.6% of sham DMSO control, $n = 6$, $P > 0.05$ with repeated measures ANOVA) (figure not shown). Two weeks after STZ injection, *ex vivo* glucose uptake in the diabetic cortex amounted to 83.2 ± 6.8% of sham DMSO control ($P < 0.05$), which was mitigated by ACEA (93.2 ± 9.8% of sham DMSO control, $n = 6$, $P > 0.05$) (figure not shown). Additionally, the CB_1R-selective neutral antagonist, O-2050 (500 nM) exacerbated the impairment of glucose uptake to −24.8 ± 7.3% compared to sham DMSO ($P < 0.05$), and this further decrease was almost significantly different from the respective STZ DMSO control ($P = 0.06$) (Fig. 1A). Four weeks post-STZ injection, glucose uptake was no longer statistically different from the sham DMSO value, and thus, WIN55212–2 also failed to further modulate glucose uptake in the STZ group (Fig. 1B). Intriguingly, acute CB_1R blockade significantly reduced glucose uptake by 22.7 ± 6.8% ($n = 6$, $P < 0.05$ vs. both sham and STZ DMSO controls). Altogether, these data suggest that the CB_1R gains a transient role in cortical glucoregulation under insulinopenia. When the slices from the T1D rats were challenged with high K^+ 2 and 4 weeks post-injection, they tended to take up almost significantly more glucose than the sham slices (Fig. 1D), but this tendency was lost after 8 weeks in T1D. In fact, 8 weeks post-STZ-injection, neither basal nor high-K^+-stimulated glucose uptake was different from the sham slices, and neither WIN55212–2 nor O-2050 (Fig. 1C), nor ACEA (3 μM; $n = 6$; figure not shown) affected glucose uptake in the two cohorts.

3.2. Dissipative glucose metabolism in frontocortical slices from diabetic rats

In the above set of experiments, we simultaneously measured the accumulation of [^{3}H]DG and the [^{14}C] label from [^{14}C]$_6$-glucose. Since the latter tracer is metabolized much faster than the former, the difference in [^{3}H] vs. [^{14}C] contents roughly measures the dissipative metabolism of glucose in the slice (for details see Lemos et al. (2012) and Supplemental

File). Dissipative metabolism was not statistically different among the three groups of sham animals. As expected, high-K^+-depolarization strongly augmented glucose metabolism in all groups of animals as gauged by the strong reduction in [^{14}C] content as compared to the [^{3}H] content, and there was a tendency too for a greater metabolic rate in the diabetic rats ($P > 0.05$) (Fig. 2). Furthermore, CB_1R activation and blockade had no significant effect on the metabolism of glucose in the slices from the 6 groups of rats (Fig. 2), although WIN55212–2 almost significantly stimulated glucose metabolism after 8 weeks in diabetes (Fig. 2C; $P > 0.05$).

These data suggest that chronic insulinopenia affects basal glucose uptake in the frontal cortex. We then asked if resting and high-K^+-depolarization-evoked glucose uptake and metabolism are subject to modulation by either insulin or cannabinoids, but more importantly, by the combination of insulin with cannabinoid agonists and antagonist, in cortical slices of ad libitum fed, 16-hour fasted (*i.e.* acutely insulinopenic) and in T1D rats. The outcome of that assay is presented in the Supplemental File (Section 2.2. and Supplemental Table 1), as we judged that those data did not add groundbreaking information to the present study.

3.3. CB_1R density and expression in the diabetic cortex

Our above functional data suggest a gain-of-function for the CB_1R in the early phase of T1D. Previous studies assessing CB_1R density in the brain of diabetic rats and mice have found contrasting results, depending on the duration of T1D after STZ-injection until sacrifice and the brain area in question (Duarte et al., 2007; Díaz-Asensio et al., 2008; de Morais et al., 2016; Moura et al., 2019). We now evaluated CB_1R immunoreactivity by Western blotting, analyzing the selective band at ~52 kDa (Bitencourt et al., 2015) in prefrontocortical homogenates 2, 4 and 8 weeks after STZ injection. We found a significant increase (24.5 ± 9.0%) in CB_1R density after 2 weeks of diabetes ($n = 6$, $P < 0.05$; Fig. 3AB) as compared to the respective sham animals. Two weeks later, this increase in CB_1R density was surprisingly inverted into an overt 30.5 ± 5.8% reduction ($n = 6$, $P < 0.01$; Fig. 3AB). By the end of the 8-week period with diabetes, there was no significant alteration in CB_1R density ($n = 6$, $P > 0.05$; Fig. 3AB). We also had access to frontocortical tissue of eight 5-month-old type-2 diabetic Goto-Kakizaki (GK) rats and ten age-matched controls, in which we observed a significant, on average 15.0% reduction in CB_1R density at 20 and 30 μg protein loads ($P < 0.05$; Fig. 3C). Finally, we divided our remaining frontocortical tissues from all the cohorts so that the material from the 2-week- and 8-week-diabetic animals was further analyzed by Western-blotting, while the 4-week-diabetic as well as the GK rat tissue was subjected to PCR analysis for CB_1R expression. The real-time PCR analysis normalized to the constitutive expression of β-actin mRNA showed that CB_1R mRNA expression was not statistically different either in the 4-week-diabetic or in the GK rats, as compared to their respective controls ($P > 0.05$; Fig. 3D).

3.4. Insulin receptor and IGF-1 receptor densities and patterns of GSK3 phosphorylation

Insulin receptor and IGF-1 receptor immunoreactivities at the expected 95 kDa molecular weight remained unaffected by 2 or 8 weeks with T1D (Fig. 4AB). Glycogen synthase kinase 3α and β isoforms are downstream targets of both the CB_1R (Solymosi and Köfalvi,

2017) and the insulin/IGF-1 receptors (Beurel et al., 2015). We now measured the phospho-Ser21 vs. total GSK3α immunoreactivity at 51 kDa and the phospho-Ser9 vs. total GSK3β immunoreactivity at 47 kDa and observed that the former decreased by 17.4 ± 4.1% ($n = 6$, $P < 0.01$) 2 weeks after STZ injection, but it was no longer significantly different from sham levels after 8 weeks with diabetes (Fig. 4CD), while GSK3β phosphorylation was initially at the sham level, but at the end of the 8-week period, it significantly increased by 19.5 ± 7.2% ($n = 6$, $P < 0.05$; Fig. 4CD).

4. Discussion

We here report a transient reduction of basal glucose uptake and its recovery in a CB_1R-dependent fashion, in the frontal cortex of rats in the first weeks after T1D induction. We also found biphasic changes in CB_1R receptor protein levels and GSK3 signaling. These changes appear counter-regulatory and sequential. Namely, after 2 weeks with T1D, the CB_1R showed an increased density and a gain-of-function, as inferred from the stimulatory effect of the cannabinoid agonist, WIN55212–2. After 4 weeks with T1D, the reduced CB_1R density seemed to be compensated by increased endocannabinoid signaling to recover basal glucose uptake rates, as deduced from the inhibitory effect of the CB_1R-selective neutral antagonist which was unseen in sham rats. Notably, this is the first report of an involvement of CB_1Rs in glucose uptake in acute brain slices, linked to our previous observation that CB_1Rs inhibit mitochondrial intermediary metabolism in astrocytes and neurons (Duarte et al., 2012). Finally, by the end of the 8^{th} week with T1D, the endocannabinoid-CB_1R axis was no longer involved in glucose uptake, and CB_1R levels returned to normal.

One may note that WIN55212–2 is a non-selective agonist of both the cannabinoid CB_1 and CB_2 receptors (Solymosi and Köfalvi, 2017). Even though the CB_2R has been occasionally shown to modulate neuronal functions (e.g. Andó et al., 2012), the CB_1R is believed to have predominant roles in marihuana's psychoactivity as well as in brain physiology and pathology (Katona and Freund, 2012; Araque et al., 2017; Fernández-Ruiz 2019). The use of the CB_1R-selective agonist, ACEA and the CB_1R-selective antagonist, O-2050 also modulated glucose uptake, underpinning the involvement of the CB_1R in our model.

Although insulin and IGF-1R levels remained constant at least 2 and 8 weeks after T1D induction, phospho-GSK3α levels were lower at the first time-point. We previously reported that CB_1R-selective ligands control GSK3α phosphorylation in acute hippocampal slices (Lemos et al., 2012). Here we found that two weeks after T1D induction, GSK3α phosphorylation at Ser21 was significantly decreased, which could have contributed to a compensatory increase in CB_1R density. In contrast, in the above paper we found no direct control by cannabinoids on GSK3β phosphorylation at Ser9, and this is in agreement with the present findings: while GSK3α phosphorylation and CB_1R functioning both became "normal" again after 8 weeks with T1D, phospho-(Ser9)-GSKβ levels were independently increased. Clearly, the dynamic interactions among CB_1R, insulin and their common downstream targets are complex and the present data only provides evidence for their involvement in the control of glucose metabolism in the frontal cortex at the early phase of T1D.

While most complications in T1D patients arise from the recurrent insulin administration as well as from unawareness of hypoglycemia rather than from chronic insulinopenia and hyperglycemia, even in the absence of microvascular complications, lower spontaneous activity is detected in the default mode network, especially in the frontal cortex of T1D patients (Xia et al., 2018). Brain glucose uptake is also smaller in both T1D patients and STZ-injected diabetic rats under hyperglycemic clamp, though there was no alteration of intermediary glucose metabolism in rats (Hwang et al., 2018). Among T1D patients, hypoglycemia-unaware patients exhibit further compromised cerebral glucose uptake at euglycemia and hypoglycemia (Cranston et al., 2001) despite the preserved transport of glucose through the blood-brain barrier (Duarte, 2015). Taken that impaired cerebral energy metabolism is associated with accelerated brain aging (de Ceballos and Köfalvi, 2017; Zilberter and Zilberter, 2017), it is evident that these complications of T1D have deleterious effects on brain microstructure (Yoon et al., 2018), leading to cognitive decline (Ryan et al., 2016).

Similarly to human T1D patients but to a much greater extent, rodent models also exhibit neuroglycopenia up to −50% of control in brain areas such as the frontal cortex, without significant alterations in cerebral blood flow (Jakobsen et al., 1987; Mooradian and Morin, 1991). Since we could recapitulate the reduced glucose uptake in resting slices in the present study, and in both resting and high-K^+-stimulated brain slices of diabetic mice, we can safely conclude that glucose uptake is impaired in brain cells in T1D. This cerebral dysmetabolism in rodent T1D models is associated with impaired acquisition and retention of memory, impaired spatial, working and reference memories, depressive behaviour and cognitive deficits (Baydas et al., 2003; de Morais et al., 2016; Lin et al., 2018), and at the cellular and molecular level, with monoaminergic dysbalance (de Morais et al., 2016; Lin et al., 2018), altered neural cell adhesion molecule expression (Baydas et al., 2003), hampered hippocampal neurogenesis, impaired synaptic plasticity, neuroinflammation, tau hyperphosphorylation and oxidative stress (Stranahan et al., 2008; Duarte, 2015; de Morais et al., 2016; Elahi et al., 2016). Whether apoptosis occurs in the brain in response to systemic STZ injection is under debate (*e.g.* Guven et al., 2009; vs. Hao et al., 2019), but transient changes in neural proliferation and apoptosis, which are tightly controlled by the CB_1R (Rodrigues et al., 2019), could certainly contribute to dysmetabolism.

Insulin and IGF-1 receptors are widely distributed in the mammalian brain (Duarte et al., 2012). Cerebral insulin receptors play a major role in the regulation of the energy metabolism of the whole body (Brüning et al., 2000; Varela and Horvath, 2012). Insulin receptor activation can also stimulate local and global rates of cerebral glucose metabolism, but only a few studies have documented these findings *in vivo* in humans (Bingham et al., 2002) and rats (McNay et al., 2010). In acute cortical slices, we could not demonstrate an impact of insulin in glucose uptake and metabolism (see Supplemental Table 1), which is in accordance with a previous study in cortical slices (Abdul-Ghani et al., 2007), but is in contrast to studies using neuronal and astrocytic cell cultures (Clarke et al.,1984; Werner et al., 1989; Kum et al., 1992; Benomar et al., 2006). Knowing that insulin is both *de novo* synthesized and taken up from the circulation in the brain (Santos et al., 1999; Banks, 2004; Molnár et al., 2014), it is possible that a fraction of basal glucose uptake in the acute brain

slices (but not in cell cultures) comes from intrinsic insulin action, which would occlude or mask effects of exogenously added insulin.

If insulin indeed stimulates cerebral glucose uptake, it could explain the consistent reports of neuroglycopenia in both T1D animal models and T1D patients, as one would expect reduced insulin levels in the brain parenchyma under T1D. But somewhat counterintuitively, the brain increases insulin production in T1D (Havrankova et al., 1978). This could probably be a key reason for the lack of changes in cerebral insulin (and IGF-1) receptor densities seen in T1D models (Havrankova et al., 1978; Packold et al., 1979). Therefore, it is less likely that an impaired insulin signaling causes cerebral hypometabolism in T1D. Instead, our previous paper (Moura et al., 2019) reveals that the T1D CB_1R KO mice had no further impairment in glucose uptake and metabolism as compared to their healthy controls. This suggests that an impairment in CB_1R signaling is downstream to insufficient insulin signaling in the cascade leading to neuroglycopenia.

The negative role of cerebral and peripheral CB_1Rs in the genesis of metabolic syndrome, insulin resistance, obesity and T2D is well-established (Di Marzo et al., 2011; Piazza et al., 2017; Ruiz de Azua et al., 2019). Yet, surprisingly little is known about the involvement of the endocannabinoid system in the development of T1D. Interestingly, a landmark study suggests that the overactivation of CB_1Rs intrinsic to β-cells can heteromerize and inhibit local insulin receptors, leading to insulin resistance, apoptosis and consequently, T1D (Kim et al., 2012). Previous studies already addressed the effect of STZ-induced diabetes on cerebral CB_1R expression/density in rats with various outcomes. For instance, Díaz-Asensio et al. (2008) reported that 4 weeks after injecting intravenously 6–8-week-old Sprague–Dawley rats with STZ, CB_1R density remained unaffected in the cortex and hippocampus, but increased in the striatum and the hypothalamus. In 12-week-old Wistar rats, 4-week after STZ injection, CB_1R density increased in the hippocampus, while CB_1R expression, *i.e.* mRNA levels, decreased, suggesting either an accelerated translation or a post-translational modification or both (Duarte et al., 2007).

Notably, the findings by de Morais and colleagues (2016) are similar to our previous and present findings. They found that 4 weeks after an intraperitoneal STZ injection, hippocampal CB_1R density significantly increased in young adult Wistar rats, while in the prefrontal cortex, it became ~30% smaller (although $P > 0.05$). It is known that chronic hyperglycemia is sufficient to downregulate neuronal CB_1R expression in neurons (Zhang et al., 2007), but there is certainly more to it, since our diabetic rats had lower CB_1R densities only once out of the three time-points. Perhaps changes in insulin signaling, high extra- and low intracellular glucose levels, glycosylation, neuroinflammation, apoptosis and gliosis all contribute to oscillating (sub)cellular changes in CB_1R levels in T1D.

5. Concluding remarks

We previously reported in mice (Moura *et al.*, 2019) and now we found in the rat that the CB_1R is involved in cerebral hypometabolism in T1D. The present data suggest that targeting cerebral CB_1Rs in T1D could be an interesting strategy to correct neuroglycopenia. We previously proposed a set of testable hypotheses about the mechanisms underlying the

influence of CB_1Rs on hippocampal and cortical glucose uptake (Moura *et al.*, 2019). It would require a sizable effort to explore these hypotheses in animal models, including the *in vivo* injections of the diabetic animals with cannabinoids both systemically and locally in the brain, which is certainly necessary to elucidate the intricate interaction among insulin and endocannabinoid signaling in brain energy metabolism. But even without knowing the exact molecular mechanisms, preclinical tests targeting the CB_1R have already been prompted by a handful of animal studies to alleviate peripheral and central symptoms of T1D (Weiss et al., 2006, 2008; Barutta et al., 2010; Vera et al., 2012).

Supplementary Material

Refer to Web version on PubMed Central for supplementary material.

Acknowledgments

Funding: This work was financed by Portuguese national funds via FCT – Fundação para a Ciência e a Tecnologia, under projects PTDC/DTP-FTO/3346/2014 (A.K.), PTDC/SAU-NSC/110954/2009 (IT), EXCL/DTP-PIC/0069/2012 (E.C.), Centro 2020 Regional Operational Programme (CENTRO-01–0145-FEDER-000008: BrainHealth 2020) (F.I.B and F.A.A.), FEDER (QREN), through Programa Operacional Factores de Competitividade – COMPETE 2020 (POCI-01–0145-FEDER-007440), HealthyAging2020 CENTRO-01–0145-FEDER-000012-N2323P30 and UID/NEU/04539/2019 (all CNC members); as well as AG028718 and NIGMS_NIH P20GM109096 (E.C.) and EFSD ERP Microvascular Novartis Pharma (E.C.); FWF Austrian Science Fund (Grant number: M 2486; C.L.); Knut and Alice Wallenberg Foundation (J.M.N.D.); and POCI-01–0145-FEDER-03127 and La Caixa Foundation (LCF/PR/HP17/52190001) (R.A.C.).

Abbreviations:

[^{3}H]DG	[^{3}H]-2-deoxy-D-glucose
2-AG	2-arachidonoyl-glycerol
3Rs	Replacement, Refinement and Reduction of Animals in Research
ACEA	arachidonyl-2’-chloroethylamide
ARRIVE	Animals in Research: Reporting In Vivo Experiments
CB_1R(s) and CB_2R(s)	cannabinoid CB_1 and CB_2 receptor(s)
FELASA	Federation for Laboratory Animal Science Associations
GSKα/β	glycogen synthase kinase α/β
HEPES	4-(2-hydroxyethyl)-1-piperazineethanesulfonic acid
IGF-1R	insulin-like growth factor-1 receptor(s)
i.p.	intraperitoneal
[^{3}H]MG	[^{3}H]-3-O-methyl-glucose
RIPA	radioimmunoprecipitation assay

SDS-PAGE	sodium dodecyl sulphate-polyacrylamide gel electrophoresis
STZ	streptozotocin
T1/2D	type-1/2 diabetes

References

Abdul-Ghani R; Qazzaz MM; Abdul-Ghani A Effect of insulin on ^{3}H-deoxyglucose uptake into brain slices and synaptosomal preparations from different brain regions. Eur. J. Sci. Res 2007, 18, 532–540. PDF (link), pages 184–192.

Andó RD, Bíró J, Csölle C, Ledent C, Sperlágh B The inhibitory action of exo- and endocannabinoids on [^{3}H]GABA release are mediated by both CB_1 and CB_2 receptors in the mouse hippocampus. Neurochem Int 2012, 60 (2), 145–52. 10.1016/j.neuint.2011.11.012. [PubMed: 22133429]

Banks WA The source of cerebral insulin. Eur. J. Pharmacol 2004, 490, 5–12. 10.1016/j.ejphar.2004.02.040 [PubMed: 15094069]

Barutta F; Corbelli A; Mastrocola R; Gambino R; Di Marzo V; Pinach S; Rastaldi MP; Perin PC; Gruden G Cannabinoid receptor 1 blockade ameliorates albuminuria in experimental diabetic nephropathy. Diabetes 2010, 59, 1046–1054. 10.2337/db09-1336 [PubMed: 20068137]

Baydas G; Nedzvetskii VS; Nerush PA; Kirichenko SV; Yoldas T Altered expression of NCAM in hippocampus and cortex may underlie memory and learning deficits in rats with streptozotocin-induced diabetes mellitus. Life Sci 2003, 73, 1907–1916. 10.1016/S0024-3205(03)00561-7 [PubMed: 12899916]

Benomar Y; Naour N; Aubourg A; Bailleux V; Gertler A; Djiane J; Guerre-Millo M; Taouis M Insulin and Leptin Induce Glut4 Plasma Membrane Translocation and Glucose Uptake in a Human Neuronal Cell Line by a Phosphatidylinositol 3-Kinase- Dependent Mechanism. Endocrinology 2006, 147, 2550–2556. 10.1210/en.2005-1464 [PubMed: 16497805]

Benowitz NL; Jones RT; Lerner CB Depression of growth hormone and cortisol response to insulin-induced hypoglycemia after prolonged oral delta-9-tetrahydrocannabinol administration in man. J. Clin. Endocrinol. Metab 1976, 42, 938–941. 10.1210/jcem-42-5-938 [PubMed: 1270583]

Bermúdez-Silva FJ; Romero-Zerbo SY; Haissaguerre M; Ruz-Maldonado I; Lhamyani S; El Bekay R; Tabarin A; Marsicano G; Cota D The cannabinoid CB1 receptor and mTORC1 signalling pathways interact to modulate glucose homeostasis in mice. Dis. Model. Mech 2016, 9, 51–61. 10.1242/dmm.020750 [PubMed: 26563389]

Beurel E; Grieco SF; Jope RS Glycogen synthase kinase-3 (GSK3): regulation, actions, and diseases. Pharmacol. Ther 2015, 148, 114–131. 10.1016/j.pharmthera.2014.11.016 [PubMed: 25435019]

Bingham EM; Hopkins D; Smith D; Pernet A; Hallett W; Reed L; Marsden PK; Amiel SA The role of insulin in human brain glucose metabolism: an ^{18}fluoro-deoxyglucose positron emission tomography study. Diabetes 2002, 51, 3384–3390. 10.2337/diabetes.51.12.3384 [PubMed: 12453890]

Bitencourt RM; Alpár A; Cinquina V; Ferreira SG; Pinheiro BS; Lemos C; Ledent C; Takahashi RN; Sialana FJ; Lubec G; et al. Lack of presynaptic interaction between glucocorticoid and CB_1 cannabinoid receptors in GABA- and glutamatergic terminals in the frontal cortex of laboratory rodents. Neurochem. Int 2015, 90, 72–84. 10.1016/j.neuint.2015.07.014 [PubMed: 26196379]

Bowles NP; Karatsoreos IN; Li X; Vemuri VK; Wood J-A; Li Z; Tamashiro KLK; Schwartz GJ; Makriyannis AM; Kunos G; et al. A peripheral endocannabinoid mechanism contributes to glucocorticoid-mediated metabolic syndrome. Proc. Natl. Acad. Sci. U.S.A 2015, 112, 285–290. 10.1073/pnas.1421420112 [PubMed: 25535367]

Brüning JC; Gautam D; Burks DJ; Gillette J; Schubert M; Orban PC; Klein R; Krone W; Müller-Wieland D; Kahn CR Role of brain insulin receptor in control of body weight and reproduction. Science 2000, 289, 2122–2125. 10.1126/science.289.5487.2122 [PubMed: 11000114]

Clarke DW; Boyd FT; Kappy MS; Raizada MK Insulin binds to specific receptors and stimulates 2-deoxy-D-glucose uptake in cultured glial cells from rat brain. J. Biol. Chem 1984, 259, 11672–11675. [PubMed: 6384211]

Cranston I; Reed LJ; Marsden PK; Amiel SA Changes in regional brain (^{18})F-fluorodeoxyglucose uptake at hypoglycemia in type 1 diabetic men associated with hypoglycemia unawareness and counter-regulatory failure. Diabetes 2001, 50, 2329–2336. 10.2337/diabetes.50.10.2329 [PubMed: 11574416]

Curtis MJ; Bond RA; Spina D; Ahluwalia A; Alexander SPA; Giembycz MA; Gilchrist A; Hoyer D; Insel PA; Izzo AA; et al. Experimental design and analysis and their reporting: new guidance for publication in BJP. Br. J. Pharmacol 2015, 172, 3461–3471. [10.1111/bph.12856 [PubMed: 26114403]

Dalton GD; Howlett AC Cannabinoid CB_1 receptors transactivate multiple receptor tyrosine kinases and regulate serine/threonine kinases to activate ERK in neuronal cells. Br. J. Pharmacol 2012, 165, 2497–2511. 10.1111/j.1476-5381.2011.01455.x [PubMed: 21518335]

de Ceballos ML; Köfalvi A Boosting brain glucose metabolism to fight neurodegeneration? Oncotarget 2017, 8, 14273–14274. 10.18632/oncotarget.15131 [PubMed: 28184023]

de Morais H; de Souza CP; da Silva LM; Ferreira DM; Baggio CH; Vanvossen AC; Cristina de Carvalho M; da Silva-Santos JE; Bertoglio LJ; Cunha JM; et al. Anandamide reverses depressive-like behavior, neurochemical abnormalities and oxidative-stress parameters in streptozotocin-diabetic rats: Role of CB1 receptors. Eur. Neuropsychopharmacol 2016, 26, 1590–1600. 10.1016/j.euroneuro.2016.08.007 [PubMed: 27544303]

de Pasquale A; Costa G; Trovato A The influence of cannabis on glucoregulation. Bull Narc 1978, 30, 33–41.

Di Marzo V; Piscitelli F; Mechoulam R Cannabinoids and endocannabinoids in metabolic disorders with focus on diabetes. Handb. Exp. Pharmacol 2011, 75–104. 10.1007/978-3-642-17214-4_4 [PubMed: 21484568]

Díaz-Asensio C; Setién R; Echevarría E; Casis L; Casis E; Garrido A; Casis O Type 1 diabetes alters brain cannabinoid receptor expression and phosphorylation status in rats. Horm. Metab. Res 2008, 40, 454–458. 10.1055/s-2008-1065323. [PubMed: 18401837]

Dringen R; Hamprecht B Differences in glycogen metabolism in astroglia-rich primary cultures and sorbitol-selected astroglial cultures derived from mouse brain. Glia 1993, 8, 143–149. 10.1002/glia.440080302 [PubMed: 8225556]

Duarte AI; Moreira PI; Oliveira CR Insulin in central nervous system: more than just a peripheral hormone. J. Aging. Res 2012, 384017. 10.1155/2012/384017 [PubMed: 22500228]

Duarte JMN Metabolic Alterations Associated to Brain Dysfunction in Diabetes. Aging. Dis 2015, 6, 304–321. 10.14336/AD.2014.1104 [PubMed: 26425386]

Duarte JMN; Ferreira SG; Carvalho RA; Cunha RA; Köfalvi A CB_1 receptor activation inhibits neuronal and astrocytic intermediary metabolism in the rat hippocampus. Neurochem. Int 2012, 60, 1–8. 10.1016/j.neuint.2011.10.019 [PubMed: 22085448]

Duarte JMN; Nogueira C; Mackie K; Oliveira CR; Cunha RA; Köfalvi A Increase of cannabinoid CB_1 receptor density in the hippocampus of streptozotocin-induced diabetic rats. Exp. Neurol 2007, 204, 479–484. 10.1016/j.expneurol.2006.11.013 [PubMed: 17222407]

Elahi M; Hasan Z; Motoi Y; Matsumoto S-E; Ishiguro K; Hattori N Region-Specific Vulnerability to Oxidative Stress, Neuroinflammation, and Tau Hyperphosphorylation in Experimental Diabetes Mellitus Mice. J. Alzheimers Dis 2016, 51, 1209–1224. 10.3233/JAD-150820 [PubMed: 26923011]

Faik P; Morgan M; Naftalin RJ; Rist RJ Transport and accumulation of 2-deoxy-D-glucose in wild-type and hexokinase-deficient cultured Chinese-hamster ovary (CHO) cells. Biochem. J 1989, 260, 153–155. 10.1042/bj2600153 [PubMed: 2775178]

Gatley SJ; Holden JE; Halama JR; DeGrado TR; Bernstein DR; Ng CK Phosphorylation of glucose analog 3-O-methyl-D-glucose by rat heart. Biochem. Biophys. Res. Commun 1984, 119, 1008–1014. 10.1016/0006-291x(84)90874-x [PubMed: 6712659]

Goto Y; Kakizaki M The Spontaneous-Diabetes Rat: A Model of Noninsulin Dependent Diabetes Mellitus. Proc. Jpn. Acad., Ser. B 1981, 57, 381–384.

Guven A; Yavuz O; Cam M; Comunoglu C; Sevi'nc O Central nervous system complications of diabetes in streptozotocin-induced diabetic rats: a histopathological and immunohistochemical examination. Int. J. Neurosci 2009, 119, 1155–1169. 10.1080/00207450902841723 [PubMed: 19922346]

Hao L; Li Q; Zhao X; Li Y; Zhang C A long noncoding RNA LOC103690121 promotes hippocampus neuronal apoptosis in streptozotocin-induced type 1 diabetes. Neurosci. Lett 2019, 703, 11–18. 10.1016/j.neulet.2019.03.006 [PubMed: 30851305]

Havrankova J; Roth J; Brownstein MJ Concentrations of insulin and insulin receptors in the brain are independent of peripheral insulin levels. Studies of obese and streptozotocin-treated rodents. J. Clin. Invest 1979, 64, 636–642. 10.1172/JCI109504 [PubMed: 156737]

Hillard CJ, Manna S, Greenberg MJ, DiCamelli R, Ross RA, Stevenson LA, Murphy V, Pertwee RG, Campbell WB Synthesis and characterization of potent and selective agonists of the neuronal cannabinoid receptor (CB1). J. Pharmacol. Exp. Ther 1999, 289, 1427–1433. [PubMed: 10336536]

Hwang JJ; Jiang L; Rangel ES; Fan X; Ding Y; Lam W; Leventhal J; Dai F; Rothman DL; Mason GF; et al. Glycemic Variability and Brain Glucose Levels in T1DM. Diabetes 2018, db180722. 10.2337/db18-0722.

Jakobsen J; Knudsen GM; Juhler M Cation permeability of the blood-brain barrier in streptozotocin-diabetic rats. Diabetologia 1987, 30, 409–413. 10.1007/BF00292543.pdf [PubMed: 3678661]

Jourdan T; Nicoloro SM; Zhou Z; Shen Y; Liu J; Coffey NJ; Cinar R; Godlewski G; Gao B; Aouadi M; et al. Decreasing CB_1 receptor signaling in Kupffer cells improves insulin sensitivity in obese mice. Mol Metab 2017, 6, 1517–1528. 10.1016/j.molmet.2017.08.011 [PubMed: 29107297]

Kilkenny C; Browne W; Cuthill IC; Emerson M; Altman DG; NC3Rs Reporting Guidelines Working Group Animal research: reporting *in vivo* experiments: the ARRIVE guidelines. Br. J. Pharmacol 2010, 160, 1577–1579. 10.1111/j.1476-5381.2010.00872.x [PubMed: 20649561]

Kim W; Lao Q; Shin Y-K; Carlson OD; Lee EK; Gorospe M; Kulkarni RN; Egan JM Cannabinoids induce pancreatic β-cell death by directly inhibiting insulin receptor activation. Sci. Signal 2012, 5, ra23. 10.1126/scisignal.2002519 [PubMed: 22434934]

Kipnis DM; Helmreich E; Cori CF Studies of Tissue Permeability IV. The Distribution Of Glucose Between Plasma And Muscle. J. Biol. Chem 1959, 234, 165–170. [PubMed: 13610914]

Kum W; Zhu SQ; Ho SK; Young JD; Cockram CS Effect of insulin on glucose and glycogen metabolism and leucine incorporation into protein in cultured mouse astrocytes. Glia 1992, 6, 264–268. 10.1002/glia.440060404 [PubMed: 1464458]

Labouèbe G; Liu S; Dias C; Zou H; Wong JCY; Karunakaran S; Clee SM; Phillips AG; Boutrel B; Borgland SL Insulin induces long-term depression of ventral tegmental area dopamine neurons via endocannabinoids. Nat. Neurosci 2013, 16, 300–308. 10.1038/nn.3321 [PubMed: 23354329]

Lemos C; Valério-Fernandes A; Ghisleni GC; Ferreira SG; Ledent C; de Ceballos ML; Köfalvi A Impaired hippocampal glucoregulation in the cannabinoid CB1 receptor knockout mice as revealed by an optimized in vitro experimental approach. J. Neurosci. Methods 2012, 204, 366–373. 10.1016/j.jneumeth.2011.11.028 [PubMed: 22155442]

Lin L-W; Tsai F-S; Yang W-T; Lai S-C; Shih C-C; Lee S-C; Wu C-R Differential change in cortical and hippocampal monoamines, and behavioral patterns in streptozotocin-induced type 1 diabetic rats. Iran. J. Basic Med. Sci 2018, 21, 1026–1034. 10.22038/IJBMS.2018.29810.7197 [PubMed: 30524676]

McGrath JC; Drummond GB; McLachlan EM; Kilkenny C; Wainwright CL Guidelines for reporting experiments involving animals: the ARRIVE guidelines. Br. J. Pharmacol 2010, 160, 1573–157610.1111/j.1476-5381.2010.00873.x [PubMed: 20649560]

McNay EC; Ong CT; McCrimmon RJ; Cresswell J; Bogan JS; Sherwin RS Hippocampal memory processes are modulated by insulin and high-fat-induced insulin resistance. Neurobiol. Learn. Mem 2010, 93, 546–553. [PubMed: 20176121]

Molnár G; Faragó N; Kocsis ÁK; Rózsa M; Lovas S; Boldog E; Báldi R; Csajbók É; Gardi J; Puskás LG; et al. GABAergic neurogliaform cells represent local sources of insulin in the cerebral cortex. J. Neurosci 2014, 34, 1133–1137. 10.1523/JNEUROSCI.4082-13.2014 [PubMed: 24453306]

Mooradian AD; Morin AM Brain uptake of glucose in diabetes mellitus: the role of glucose transporters. Am. J. Med. Sci 1991, 301, 173–177. 10.1097/00000441-199103000-00004 [PubMed: 2000888]

Morgan HE; Park CR Sugar transport across muscle cell membrane Fed. Proc 1958, 17, 278.

Moura LIF; Lemos C; Ledent C; Carvalho E; Köfalvi A Chronic insulinopenia/hyperglycemia decrease cannabinoid CB_1 receptor density and impair glucose uptake in the mouse forebrain. Brain Res. Bull 2019, 147, 101–109. 10.1016/j.brainresbull.2019.01.024 [PubMed: 30721768]

Pacold ST; Blackard WG Central nervous system insulin receptors in normal and diabetic rats. Endocrinology 1979, 105, 1452–1457. 10.1210/endo-105-6-1452 [PubMed: 499083]

Piazza PV; Cota D; Marsicano G The CB_1 Receptor as the Cornerstone of Exostasis. Neuron 2017, 93, 1252–1274. 10.1016/j.neuron.2017.02.002 [PubMed: 28334603]

Pinheiro BS; Lemos C; Neutzling Kaufmann F; Marques JM; da Silva-Santos CS; Carvalho E; Mackie K; Rodrigues RJ; Cunha RA; Köfalvi A Hierarchical glucocorticoidendocannabinoid interplay regulates the activation of the nucleus accumbens by insulin. Brain Res. Bull 2016, 124, 222–230. 10.1016/j.brainresbull.2016.05.009 [PubMed: 27208730]

Rehni AK; Dave KR Impact of Hypoglycemia on Brain Metabolism During Diabetes. Mol. Neurobiol 2018, 55, 9075–9088. 10.1007/s12035-018-1044-6 [PubMed: 29637442]

Rodrigues RS; Lourenço DM; Paulo SL; Mateus JM; Ferreira MF; Mouro FM; Moreira JB; Ribeiro FF; Sebastião AM; Xapelli S Cannabinoid Actions on Neural Stem Cells: Implications for Pathophysiology. Molecules 2019, 24, pii: E1350. 10.3390/molecules24071350

Ruiz de Azua I; Lutz B Multiple endocannabinoid-mediated mechanisms in the regulation of energy homeostasis in brain and peripheral tissues. Cell. Mol. Life Sci 2019, 76, 1341–1363. 10.1007/s00018-018-2994-6 [PubMed: 30599065]

Ryan CM; van Duinkerken E; Rosano C Neurocognitive consequences of diabetes. Am. Psychol 2016, 71, 563–576. 10.1037/a0040455 [PubMed: 27690485]

Santos MS; Pereira EM; Carvaho AP Stimulation of immunoreactive insulin release by glucose in rat brain synaptosomes. Neurochem. Res 1999, 24, 33–36. [PubMed: 9973234]

Sidibeh CO; Pereira MJ; Lau Börjesson J; Kamble PG; Skrtic S; Katsogiannos P; Sundbom M; Svensson MK; Eriksson JW Role of cannabinoid receptor 1 in human adipose tissue for lipolysis regulation and insulin resistance. Endocrine 2017, 55, 839–852. 10.1007/s12020-016-1172-6 [PubMed: 27858284]

Solymosi K; Köfalvi A Cannabis: A Treasure Trove or Pandora's Box? Mini Rev Med Chem 2017, 17, 1223–1291. 10.2174/1389557516666161004162133 [PubMed: 27719666]

Stranahan AM; Arumugam TV; Cutler RG; Lee K; Egan JM; Mattson MP Diabetes impairs hippocampal function through glucocorticoid-mediated effects on new and mature neurons. Nat. Neurosci 2008, 11, 309–317. 10.1038/nn2055 [PubMed: 18278039]

Szkudelski T The mechanism of alloxan and streptozotocin action in B cells of the rat pancreas. Physiol Res 2001, 50, 537–546. http://www.biomed.cas.cz/physiolres/pdf/50/50_537.pdf [PubMed: 11829314]

Varela L; Horvath TL Leptin and insulin pathways in POMC and AgRP neurons that modulate energy balance and glucose homeostasis. EMBO Rep 2012, 13, 1079–1086. 10.1038/embor.2012.174 [PubMed: 23146889]

Vera G; López-Miranda V; Herradón E; Martín MI; Abalo R Characterization of cannabinoid-induced relief of neuropathic pain in rat models of type 1 and type 2 diabetes. Pharmacol. Biochem. Behav 2012, 102, 335–343. 10.1016/j.pbb.2012.05.008 [PubMed: 22609797]

Weiss L; Zeira M; Reich S; Har-Noy M; Mechoulam R; Slavin S; Gallily R Cannabidiol lowers incidence of diabetes in non-obese diabetic mice. Autoimmunity 2006, 39, 143–151. 10.1080/08916930500356674 [PubMed: 16698671]

Weiss L; Zeira M; Reich S; Slavin S; Raz I; Mechoulam R; Gallily R Cannabidiol Arrests Onset of Autoimmune Diabetes in NOD Mice. Neuropharmacology 2008, 54, 244–249. 10.1016/j.neuropharm.2007.06.029 [PubMed: 17714746]

Werner H; Woloschak M; Adamo M; Shen-Orr Z; Roberts CT; LeRoith D Developmental regulation of the rat insulin-like growth factor I receptor gene. Proc. Natl. Acad. Sci. U.S.A 1989, 86, 7451–7455. 10.1073/pnas.86.19.7451 [PubMed: 2477843]

Xia W; Chen Y-C; Luo Y; Zhang D-F; Chen H; Ma J; Yin X Decreased Spontaneous Brain Activity and Functional Connectivity in Type 1 Diabetic Patients Without Microvascular Complications. Cell. Physiol. Biochem 2018, 51, 2694–2703. 10.1159/000495960 [PubMed: 30562754]

Yoon S; Kim J; Musen G; Renshaw PF; Hwang J; Bolo NR; Kim JE; Simonson DC; Weinger K; Ryan CM; et al. Prefronto-temporal white matter microstructural alterations 20 years after the diagnosis of type 1 diabetes mellitus. Pediatr. Diabetes 2018, 19, 478–485. 10.1111/pedi.12574 [PubMed: 28929564]

Zhang F; Hong S; Stone V; Smith PJW Expression of cannabinoid CB_1 receptors in models of diabetic neuropathy. J. Pharmacol. Exp. Ther 2007, 323, 508–515. 10.1124/jpet.107.128272 [PubMed: 17702901]

Zilberter Y; Zilberter M The vicious circle of hypometabolism in neurodegenerative diseases: Ways and mechanisms of metabolic correction. J. Neurosci. Res 2017, 95, 2217–2235. 10.1002/jnr.24064 [PubMed: 28463438]

Highlights

- Frontocortical glucose uptake is smaller early after type-1 diabetes (T1D) induction
- The recovery from neuroglycopenia in T1D is cannabinoid CB_1 receptor-dependent
- T1D induction is followed by a biphasic change in CB_1R levels and insulin signaling

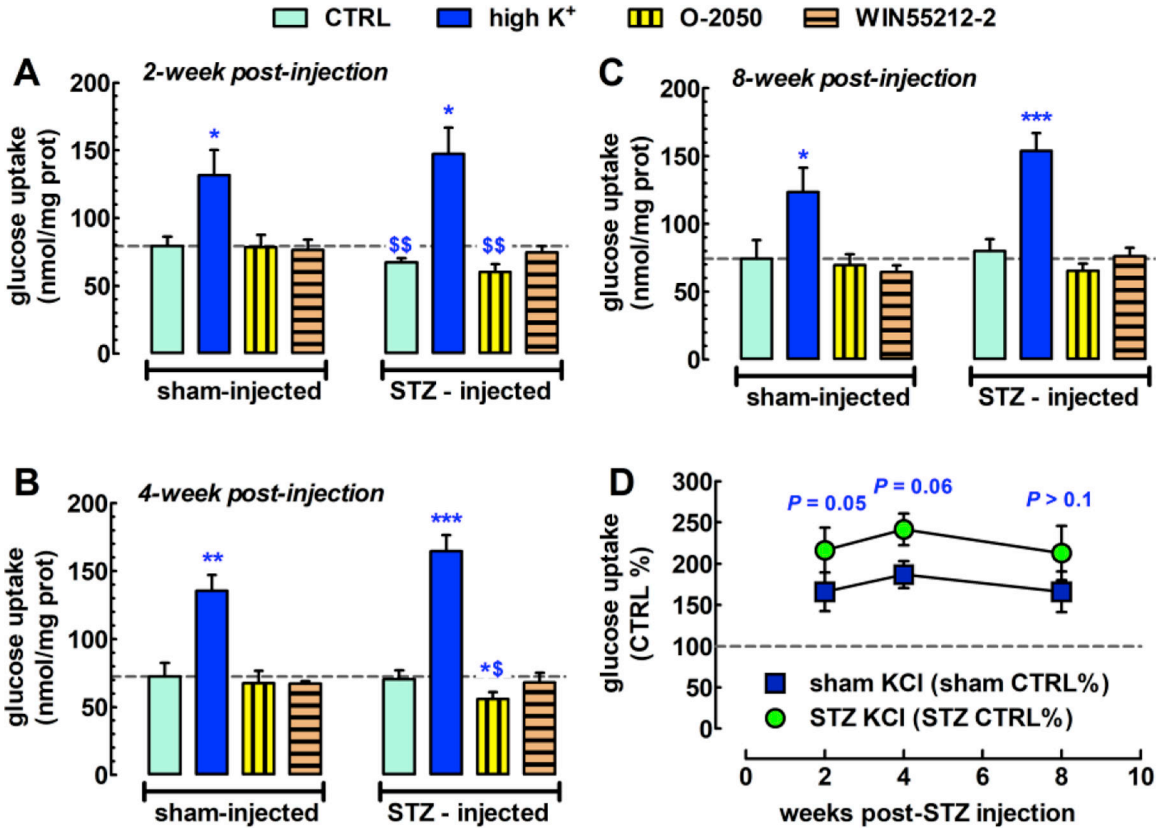

Fig. 1.

STZ-induced insulinopenia impairs resting glucose uptake in a CB_1R-dependent fashion. (**A**) Two-weeks after T1D induction, resting glucose uptake was significantly lower than in the sham animals (n=14; $P < 0.01$), which was further decreased by CB_1R blockade with the neutral CB_1R antagonist, O-2050 (500 nM), although non-significantly ($P = 0.058$ vs. STZ control). This reduction was recovered to the sham control value in the presence of the synthetic cannabinoid, WIN55212–2 (500 nM) ($P > 0.05$ vs. sham control). (**B**) After 4 weeks with T1D, resting glucose uptake was no longer different from the sham value ($P > 0.05$), and hence, WIN55212–2 failed to stimulate glucose uptake further, but O-2050 uncovered a significant reduction as compared to either the sham or the respective diabetic DMSO control value (n=8; $P < 0.05$). (**C**) After 8 weeks with T1D, the metabolic disturbances fully recovered, and neither the activation nor the blockade of the CB_1R affected glucose uptake (n=8; $P > 0.05$). (**D**) The difference in the amplitudes of high K^+-stimulated glucose uptake normalized to the appropriate sham or STZ control was tendentiously at the border of significance between sham and diabetic animals. Note that all four chambers had identical osmotic condition (achieved with extra NaCl or KCl) and 0.1% DMSO as a vehicle. All bars and symbols represent mean + or ± S.E.M.; *$P < 0.05$, **$P < 0.01$, ***$P < 0.001$ vs. the respective control (sham or STZ), and $^{\$}P < 0.05$, $^{\$\$}P < 0.01$ vs. sham control from the same experiment in pairwise arrangement, as assessed with Repeated Measures ANOVA following by Bonferroni's post-hoc test for selected pairs of data sets.

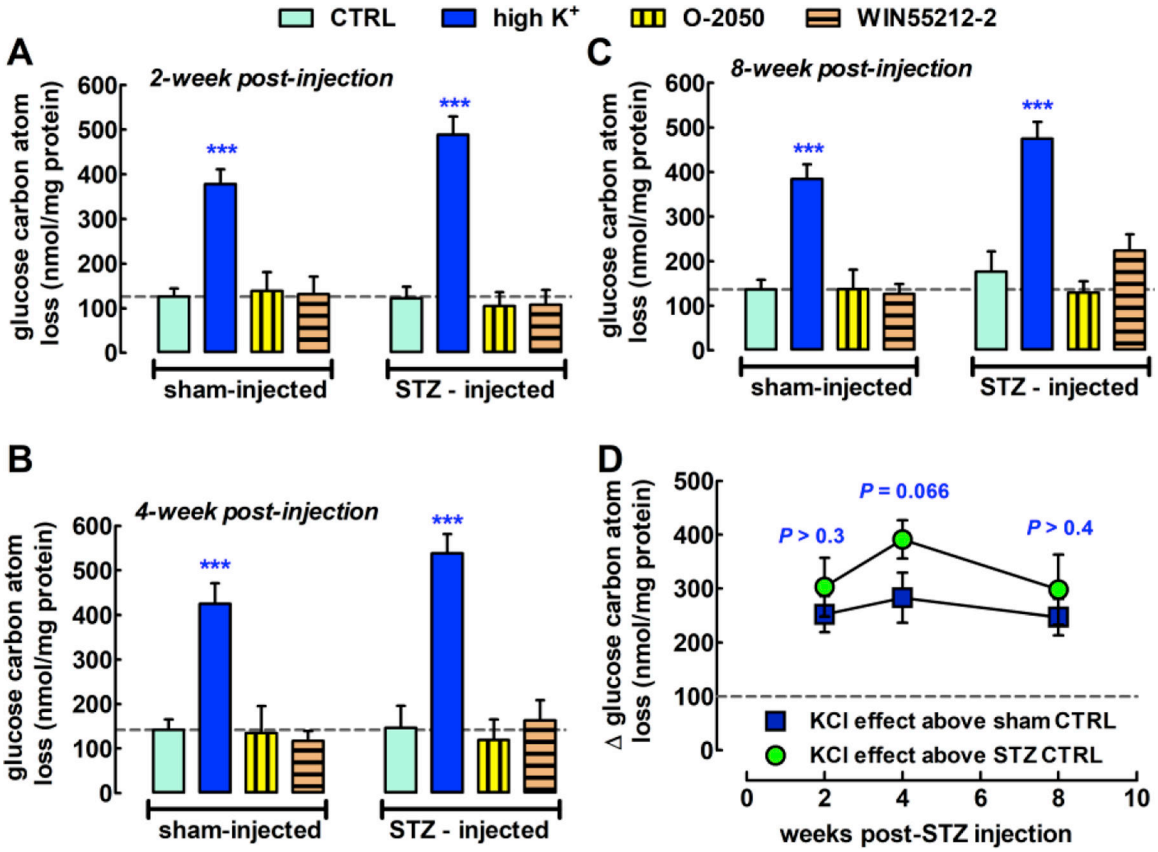

Fig. 2.

Dissipative glucose metabolism is not affected by chronic insulinopenia or acutely by CB_1R ligands or the two combined in the rat frontal cortex. (**A**) Two-weeks, (**B**) four weeks and (**C**) eight weeks after T1D induction, resting glucose uptake was similar between the two cohorts (n=14, 8 and 8, respectively; $P < 0.05$), and only responded significantly to high-K^+ treatment ($P < 0.001$). (**D**) The amplitude of response to depolarization was also similar between the two groups, although there was a non-significant tendency (n=14, 8 and 8, respectively; $P > 0.05$) for greater [^{14}C] release in the slices prepared from the diabetic rats. All bars and symbols represent mean +/± S.E.M.; ***$P < 0.001$ vs. the respective sham or STZ control, from the same experiment in pairwise arrangement, as assessed with Repeated Measures ANOVA following by Bonferroni's post-hoc test for selected pairs of data sets.

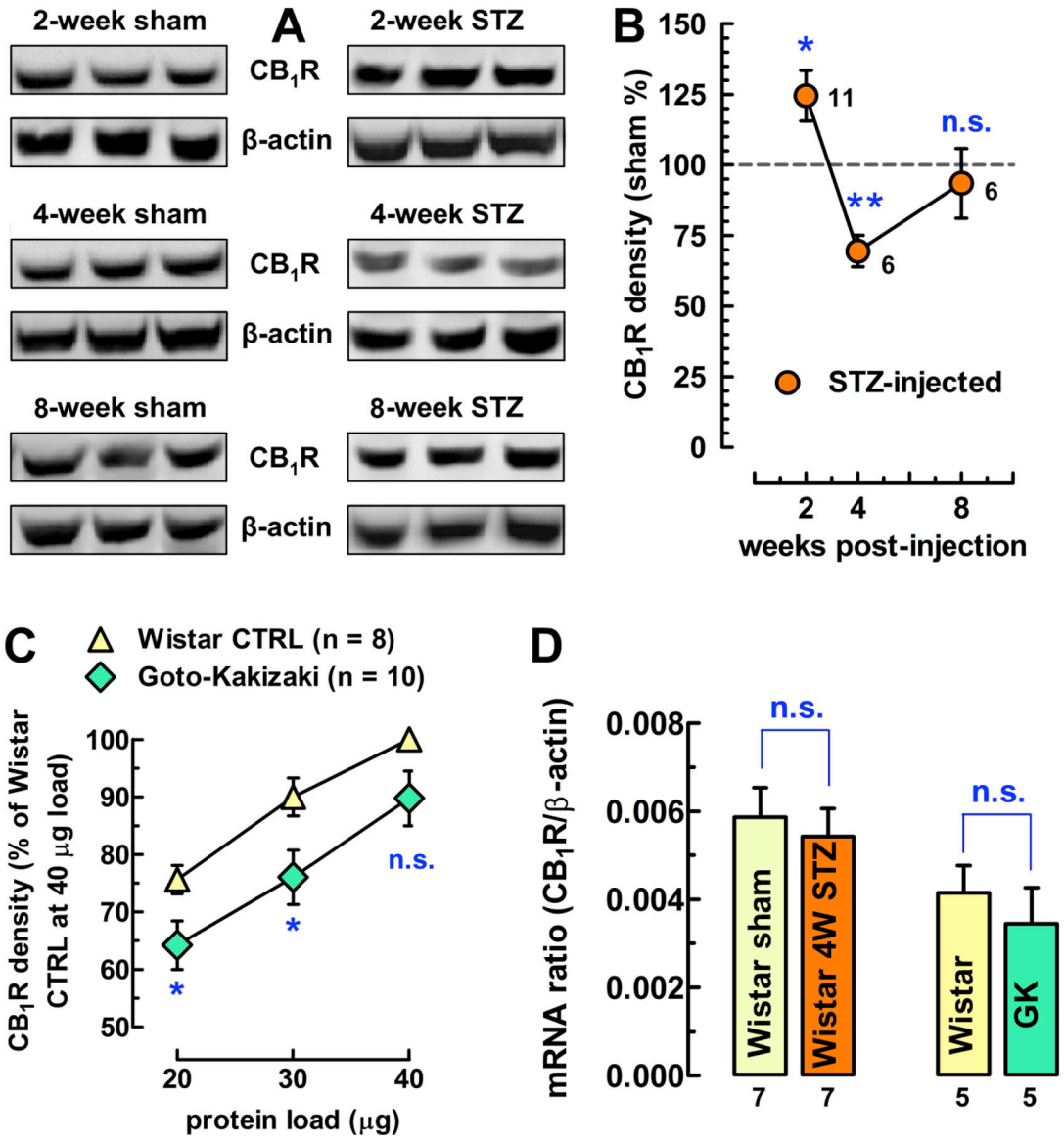

Fig. 3.

The cortical density rather than the expression of the CB_1R is affected by T1D and T2D. (**A**) representative blots showing the 53 kDa CB_1R immunoreactivity and the 42 kDa β-actin immunoreactivity at 30 μg protein load, in diabetic rats at 2, 4 and 8 weeks after STZ-injection, and in the corresponding sham-injected animals. Panel (**B**) shows the mean ± S.E.M. of CB_1R immunoreactivities normalized to β-actin (CB_1R densities), and expressed to the same normalized data obtained in the respective sham animals. (**C**) CB_1R densities (mean ± S.E.M) are significantly lower in the type-2 diabetic GK rats (n = 10) than in their controls (n = 8). (**D**) Bar graphs summarizing average CB_1R expression + S.E.M. in the 16 week-old sham and T1D rats as well as in the 20-week old control and GK rats. *P < 0.05 and **P < 0.01 vs. the respective sham control; n.s., not significant.

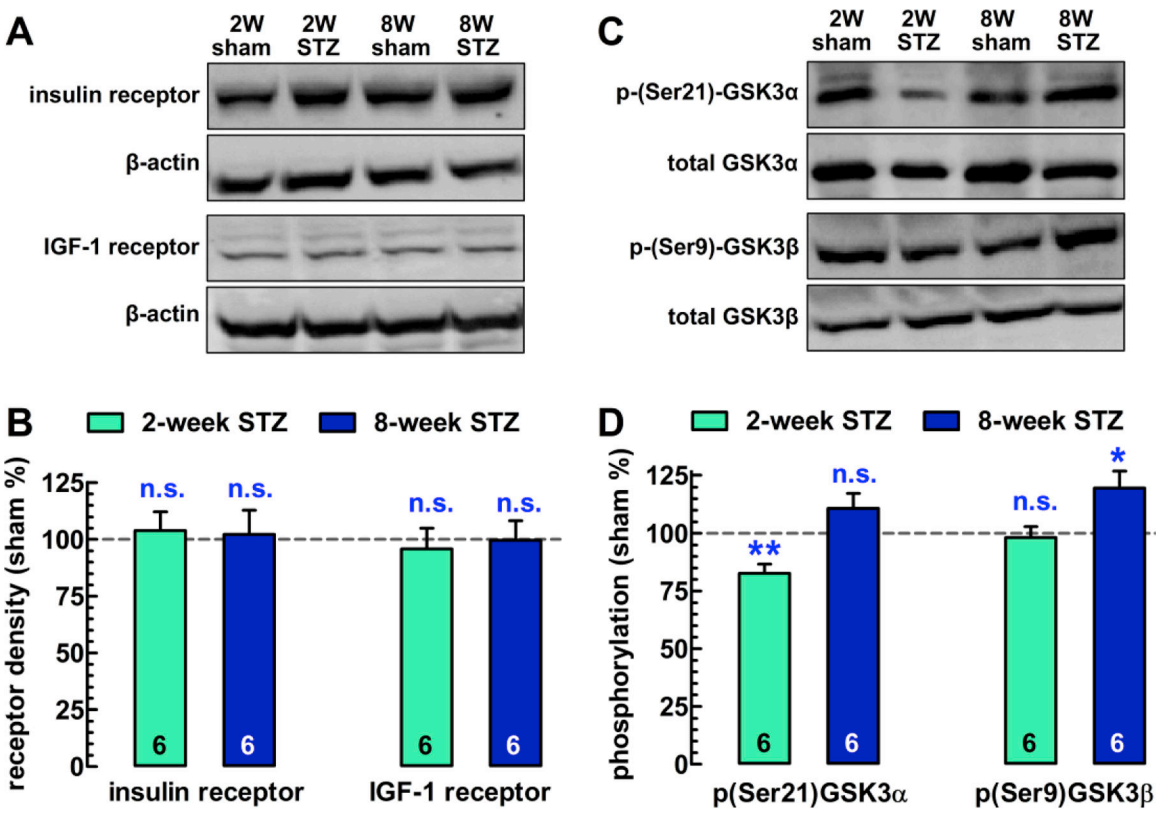

Fig. 4.

STZ-induced diabetes alters the activation of the insulin signaling pathway while leaving insulin and IGF-1R densities unaffected. (**A,C**) Representative blots and (**B,D**) the respective bar graphs showing that insulin and IGF-1 receptor densities remain unaffected after 2 and 8 weeks with T1D (as normalized to the β-actin levels). Furthermore, 2 weeks with diabetes decreases phospho(Ser21)GSK3α density while leaving phospho(Ser9)GSK3β density unaffected, but after 8 weeks with T1D, the former returns to control why the latter significantly increases. All bars represent mean + S.E.M of 6 rats; *P < 0.05, **P < 0.01 vs. sham ratios taken as 100%.

Table 1.

Primers used in the real-time PCR analysis.

	Accession number	Primer sequence	Expected product size (bp)
CB_1R (Hansson et al., 2007)	NM_012784	F 5'- AGA CCT CCT CTA CGT GGG CTC G −3' R 5'- GTA CAG CGA TGG CCA GCT GCT G −3'	314
β-actin (Peinnequin et al., 2004)	V01217	F 5'- AAG TCC CTC ACC CTC CCA AAA G −3' R 5'- AAG CAA TGC TGT CAC CTT CCC −3'	97

Table 2.

Cycling parameters for real-time and conventional PCR analysis.

Real-time PCR							
	$MgCl_2$ (mM)	Initial denaturation	Amplification				Melting curve analysis
			Denaturation	Annealing	Extension	Cycles	
CB_1R	3	95 °C, 10 m	95 °C, 10 s	62 °C, 10 s	72 °C, 14 s	40	
β-actin	3.5	95 °C, 10 m	95 °C, 10 s	61 °C, 5 s	72 °C, 4 s	45	
Conventional PCR							
	$MgCl_2$ (mM)	Initial denaturation	Amplification				Elongation
			Denaturation	Annealing	Extension	Cycles	
CB_1R	1.5	95 °C, 5 m	95 °C, 1 m	59 °C, 1 m	72 °C, 1 m	45	72 °C, 4 m
β-actin	1.5	95 °C, 5 m	95 °C, 1 m	56 °C, 1 m	72 °C, 1 m	45	72 °C, 4 m